

JAN 10 1979

REPORT

RECEIVED
OAK RIDGE NATIONAL LABORATORY

281A24

OAK RIDGE NATIONAL LABORATORY

OPERATED BY
UNION CARBIDE CORPORATION
NUCLEAR DIVISION



POST OFFICE BOX X
OAK RIDGE, TENNESSEE 37830

ORNL/MIT-274

DATE: April 26, 1978

SUBJECT: Radiative Heat Transfer in a 19-Pin Sodium-Voided Bundle

Authors: M. Machbitz, B. Budiman, and Y.Y. Roberts

Consultant: J.T. Han

ABSTRACT

A theoretical study was made of the radiative heat removal capability in a 19-pin bundle simulating the fuel assemblies of the commercial-scale (217-pin) Clinch River Breeder Reactor. Pin surface temperature distributions and the maximum allowable uniform pin power (without causing cladding meltdown) were determined for a range of emissivities and duct-wall temperatures. It was concluded that radiative heat transfer ranging to 0.1 kW/ft was comparable to free convection ranging to 0.02 kW/ft, and was lower than that of forced convection cooling to 2.17 kW/ft by the sodium vapor.

Oak Ridge Station
School of Chemical Engineering Practice
Massachusetts Institute of Technology
S.M. Senkan, Director

Printed in the United States of America. Available from
National Technical Information Service
U.S. Department of Commerce
5285 Port Royal Road, Springfield, Virginia 22161
Price: Printed Copy \$4.50; Microfiche \$3.00

This report was prepared as an account of work sponsored by an agency of the United States Government. Neither the United States Government nor any agency thereof, nor any of their employees, contractors, subcontractors, or their employees, makes any warranty, express or implied, nor assumes any legal liability or responsibility for any third party's use or the results of such use of any information, apparatus, product or process disclosed in this report, nor represents that its use by such third party would not infringe privately owned rights.

Contents

	<u>Page</u>
1. Summary	4
2. Introduction	4
2.1 Background	4
2.2 Objectives	6
3. Procedure	6
3.1 Theory	6
3.2 Other Modes of Heat Transfer	12
3.3 Radial Temperature Distribution of the Center Pin	13
4. Results and Discussion	15
4.1 Pin Surface Temperature Distributions	15
4.2 Comparison of Radiative Heat Transfer with Other Modes of Heat Transfer	23
4.3 Radial Temperature Distribution of the Center Pin	23
5. Conclusions	28
6. Recommendations	28
7. Acknowledgments	28
8. Appendix	29
8.1 Additional Results	29
8.2 View Factors	35
8.3 Computer Program	39
8.4 Sample Heat Transfer Calculations	40
8.5 Nomenclature	42
8.6 Literature References	44

1. SUMMARY

One possible core-disruptive accident in Liquid Metal Cooled Fast Breeder Reactor (LMFBR) operation is the boiling off of the primary liquid sodium. To better understand the consequences of this in the full-scale 217-plus fuel assemblies, a theoretical study was made for a 19-pin bundle. Given the maximum allowable pin surface temperature of 1644 K and various duct-wall temperatures of 589 to 808 K, temperature distributions were generated using the net radiation method for different values of uniform pin power (100 to 20,000 W/m²).

It was found that the uniform-radiosity assumption led to poor results. In considering nonuniform radiosity, dividing the pin bundle into three concentric hexagons gave more realistic results than dividing the individual pin surfaces into thirds.

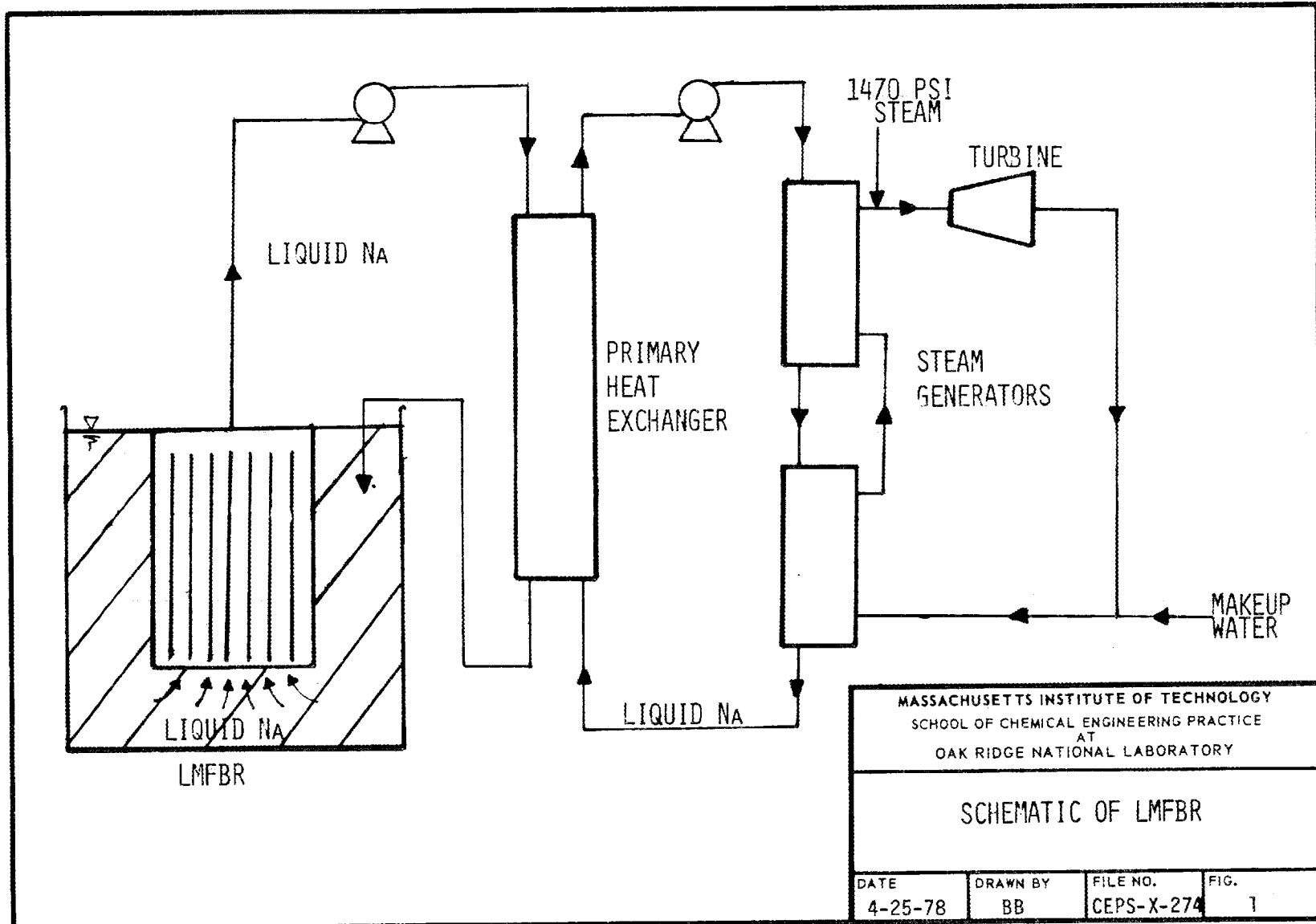
Heat transfer rates were also determined for free and forced convection of the sodium vapor and flow boiling of the liquid sodium. Radiative heat transfer rates ranging to 0.10 kW/ft were found to lie between free- and forced-convection rates, but were at least three orders of magnitude below that of flow-boiling heat transfer. It was found that at steady-state conditions, fuel meltdown takes place only at the extreme conditions of full power of 1.792×10^6 W/m² and liquid sodium temperatures above 1200 K.

2. INTRODUCTION

2.1 Background

One possible core-disruptive accident considered in the accident analysis for a Liquid Metal Cooled Fast Breeder Reactor (LMFBR) is the boiling off of the primary liquid sodium due to a blockage or rupture in the sodium line or failure of the sodium pumps (see Fig. 1). With the subsequent loss of forced convection cooling by the sodium liquid, first the fuel-pin cladding (316 stainless steel) and then the PuO₂-UO₂ fuel meltdowns would result (4, 5, 7, 11). In the extreme case of both liquid and gaseous sodium being voided, radiation would be the only mode of heat transfer. To arrive at this extreme case, transition regimes involving flow-boiling of the liquid sodium and free and forced convection of the sodium vapor must be passed.

A 19-pin reactor-core bundle was developed to simulate the fuel assemblies of the commercial-scale (217-pin) Clinch River Breeder Reactor (CRBR). Hence, radiative heat transfer characteristics of this unit were examined. The maximum temperature of the center pin surface was set at 2500°F, the melting point of the 316 stainless steel cladding. This is in contrast to the maximum set by previous workers who assumed that pin failure occurs at 5072°F, corresponding to the melting point of the PuO₂-UO₂ fuel (3, 6).



2.2 Objectives

The objectives were:

- 1) to generate pin-surface temperature distributions as functions of pin power, emissivity, and duct-wall temperature, where the cladding temperature of the center pin is set at its melting point of 1644°K (2500°F);
- 2) to determine the maximum allowable uniform pin power generation when radiation is the only mode of heat transfer which will still avoid cladding meltdown;
- 3) to determine the steady-state radial temperature distribution in the center pin corresponding to normal LMFBR operation. This steady-state profile could then be used as the initial condition in the transient problem to realistically assess a hypothetical LMFBR accident.

3. PROCEDURE

3.1 Theory

The following classical assumptions were made in formulating the problem:

- 1) Each surface is isothermal.
- 2) The surfaces are gray, i.e., emissivities ϵ and absorptivities α are independent of wavelength.
- 3) Radiation is diffusely reflected and emitted. Application of Kirchoff's Law (18) then gives:

$$\epsilon = \alpha = 1 - \gamma \quad (1)$$

where ϵ , α , and γ are functions of the surface temperature only.

- 4) Radiosity is uniform for each surface.

The net radiation method (15, 17, 18, 19) was then used to calculate the radiant exchange between the pins. The relevant equations are:

$$q_i'' = B_i - H_i \quad (2)$$

$$q_i'' = \epsilon_i (\sigma T_i^4 - H_i) \quad (3)$$

$$H_i = \sum_{j=1}^N F_{ij} B_j \quad (4)$$

$$q_i'' = B_i - \sum_{j=1}^N F_{ij} B_j = (1 - F_{ii}) B_i - \sum_{\substack{j=1 \\ j \neq i}}^N F_{ij} B_j \quad (5)$$

$$\epsilon_i \sigma T_N^4 = B_N - (1 - \epsilon_N) \sum_{j=1}^N B_j F_{ij} \quad (6)$$

where N is the total number of surfaces in the 19-pin bundle and T_N is the temperature of the duct wall. If q_i'' and F_{ij} are known, the radiosity B_i of each of the pins can be found by using Eq. (5). Equation (6) would be used to find B_N . Then either Eq. (2) or (4) is used to calculate H_i . Finally, Eq. (3) would be used to find the unknown T_i . Then q_i'' can be found to keep the center pin at or below the melting point of the cladding. The values of T_N are shown in Table 1.

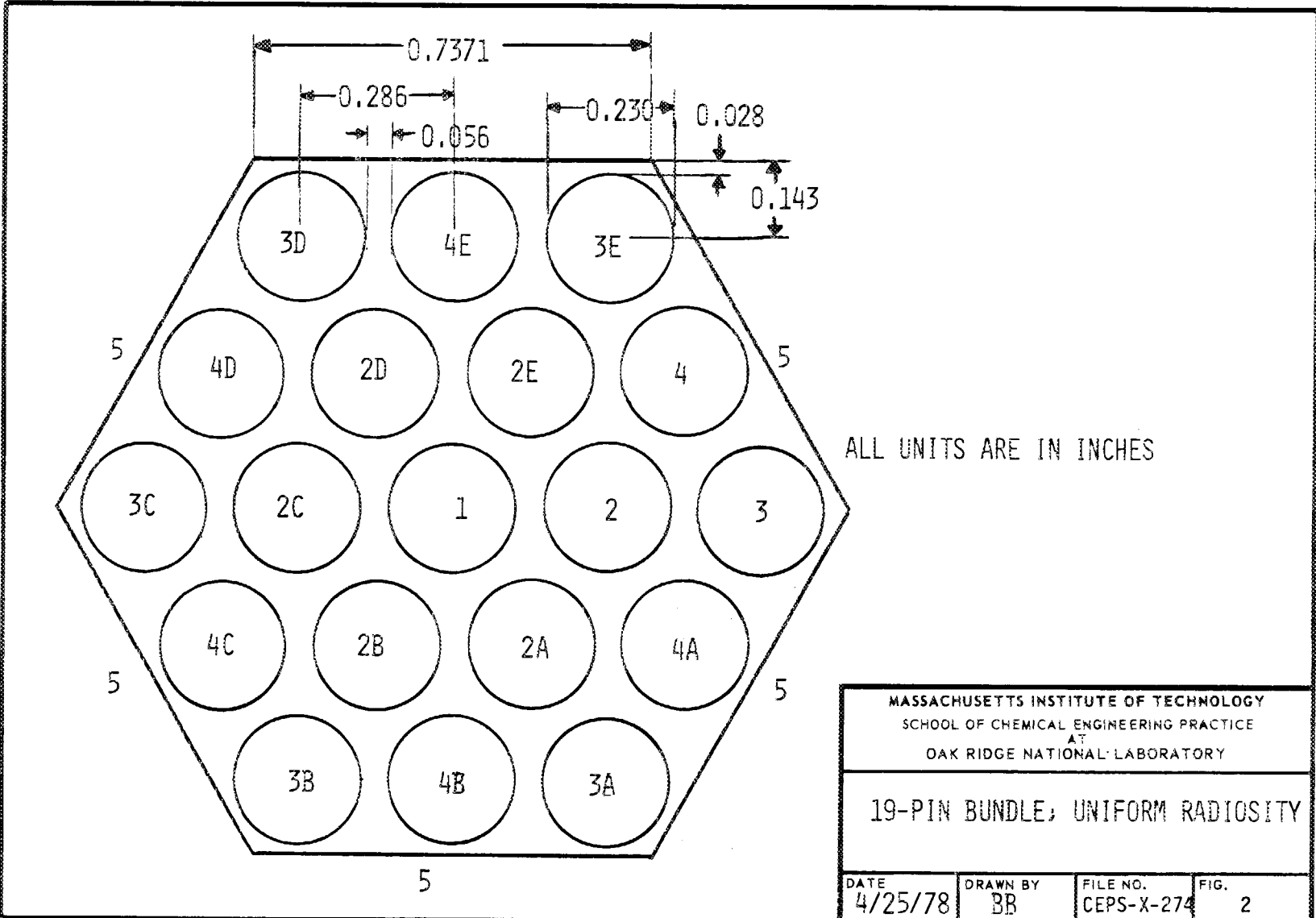
Table 1. Values of Wall Temperature Used in Calculations

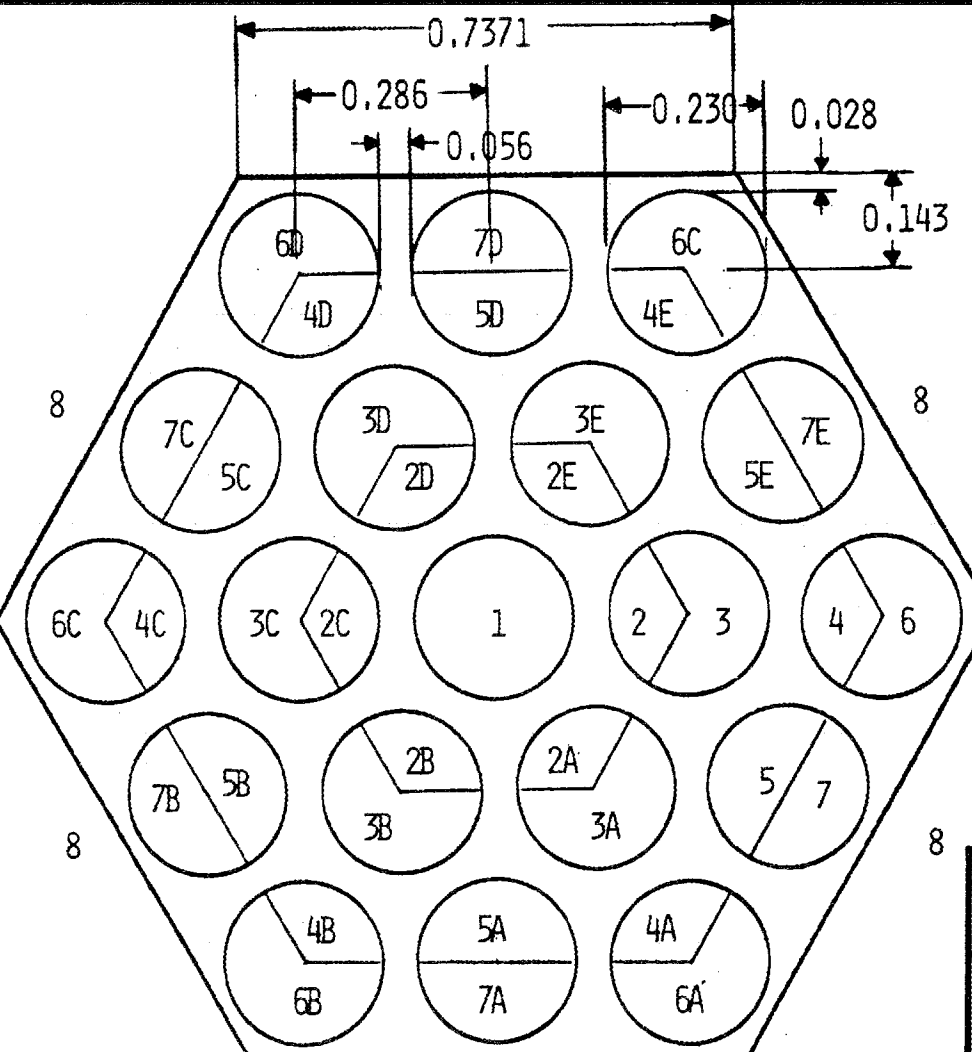
T_N	Corresponds to Sodium Temperature at:	
(°K)	(°F)	
808.15	995	outlet of CRBR core
732.00	858	outlet of FFTF* reactor core
661.00	730	inlet of CRBR core
589.00	600	inlet of FFTF reactor core

*Fast Flux Test Facility at Richland, Washington

The view factors for the three radiosity configurations shown in Figs. 2 through 4 were determined by using Hottel's crossed-string method (17, 18). Accordingly, if A_1 and A_2 are any two areas, as shown in Fig. 5, the view factor F_{12} is given by the equation

$$F_{12} = \frac{dg + ae - abcd - efg}{2A_1} \quad (7)$$





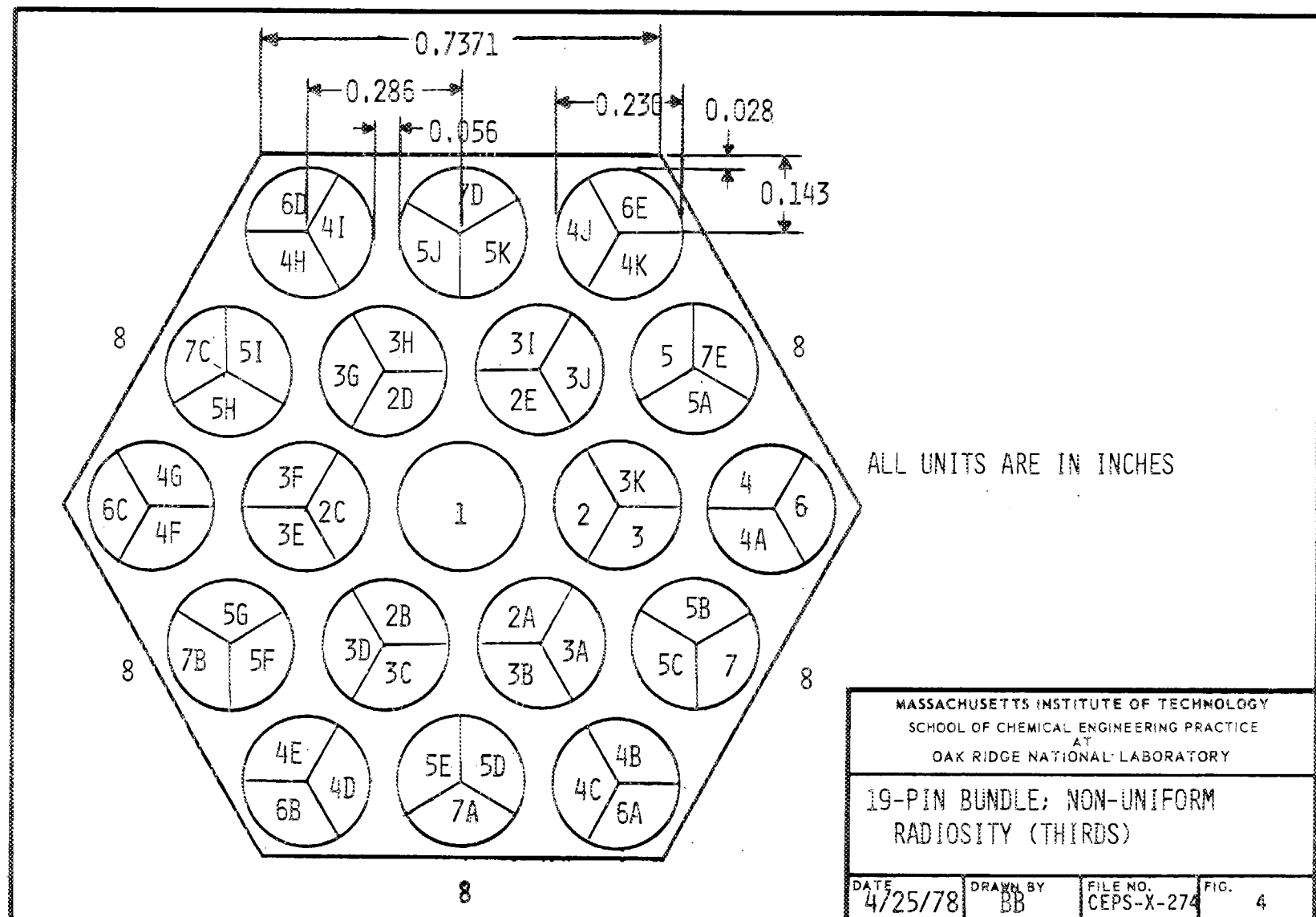
ALL UNITS ARE IN INCHES

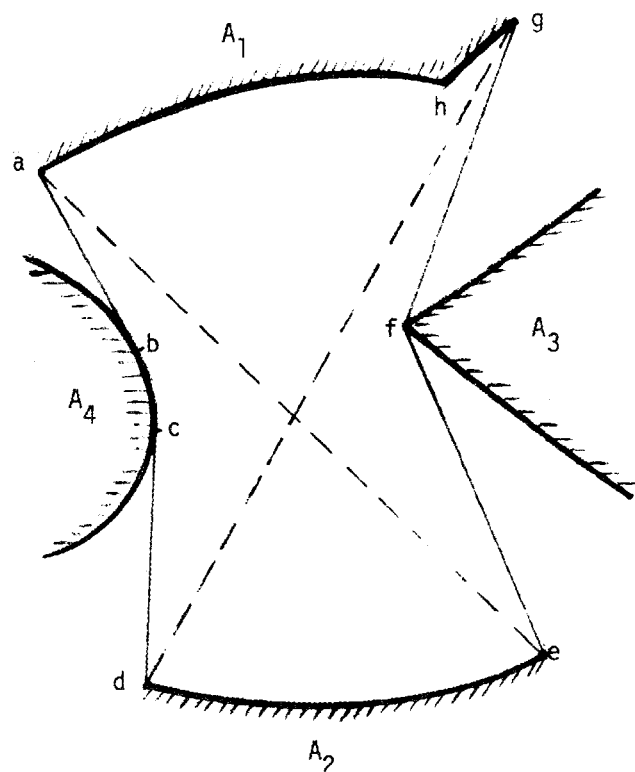
6

MASSACHUSETTS INSTITUTE OF TECHNOLOGY
SCHOOL OF CHEMICAL ENGINEERING PRACTICE
AT
OAK RIDGE NATIONAL LABORATORY

19-PIN BUNDLE; NON-UNIFORM
RADIOSITY (CONCENTRIC HEXAGONS)

DATE 4/25/78	DRAWN BY BB	FILE NO. CEPS-X-274	FIG. 3
-----------------	----------------	------------------------	-----------





MASSACHUSETTS INSTITUTE OF TECHNOLOGY
SCHOOL OF CHEMICAL ENGINEERING PRACTICE
AT
OAK RIDGE NATIONAL LABORATORY

VIEW FACTOR CALCULATION
HOTTEL'S CROSSED -STRING METHOD

DATE 4/25/78	DRAWN BY BB	FILE NO. CEPS-X-274	FIG. 5
-----------------	----------------	------------------------	-----------

The F_{ij} for the three configurations are presented in Tables 6, 7, and 8 of Appendix 8.2.

Equations (5) and (6) can be stated as:

$$q_i'' = C_{ij} B_i \quad (8)$$

where for $i \neq N$,

$$C_{ii} = 1 - F_{ii} \quad (9)$$

$$C_{ij} = -F_{ij}, \text{ for } i \neq j \quad (10)$$

$$q_i'' = \text{constant} \quad (11)$$

For $i = N$,

$$C_{Nj} = 1 - (1 - \epsilon_N) F_{Nj}, \text{ for } i = j \quad (12)$$

$$C_{Nj} = -(1 - \epsilon_N) F_{Nj}, \text{ for } i \neq j \quad (13)$$

$$q_N'' = \epsilon \sigma T_N^4 \quad (14)$$

The computer program used in solving the above set of equations is listed in Appendix 8.3.

3.2 Other Modes of Heat Transfer

Free-convection heat transfer rates of sodium vapor in the 19-pin bundles were also calculated and plotted as a function of the temperature difference between the pin surface temperature and of the sodium vapor by using the following correlation (10):

$$Nu_x = 0.508 Pr^{1/2} (0.952 + Pr)^{-1/4} (Gr_x)^{1/4} \quad Gr_x < 10^9 \quad (15)$$

Forced convection by sodium vapor was determined by using the following correlation (13) for the purpose of comparison:

$$Nu = 6 + 0.027 Re^{0.8} Pr^{0.8} \quad (16)$$

The flow boiling heat transfer for sodium liquid was also calculated using the correlation developed by Labuntsov (9):

$$Nu_b = 0.125[(Re)(Pr_\ell)]^{2/3} \quad (17)$$

Appendix 8.4 presents the details of these calculations.

3.3 Radial Temperature Distribution of the Center Pin

The equations describing heat generation and conduction (2) in the various parts of the fuel pin are (the subscripts F, H, and C denote fuel, helium, and cladding, respectively; see Fig. 6):

Fuel

$$k_F \frac{1}{r} \frac{d}{dr}(r \frac{dT}{dr}) + Q_v = 0 \quad 0 \leq r \leq r_F \quad (18)$$

Helium Gap

$$k_H \frac{1}{r} \frac{d}{dr}(r \frac{dT}{dr}) = 0 \text{ (neglecting any convection)} \quad r_F \leq r \leq r_H \quad (19)$$

Type 316 Stainless Steel Cladding

$$k_C \frac{1}{r} \frac{d}{dr}(r \frac{dT}{dr}) = 0 \quad r_H \leq r \leq r_C \quad (20)$$

The boundary conditions are:

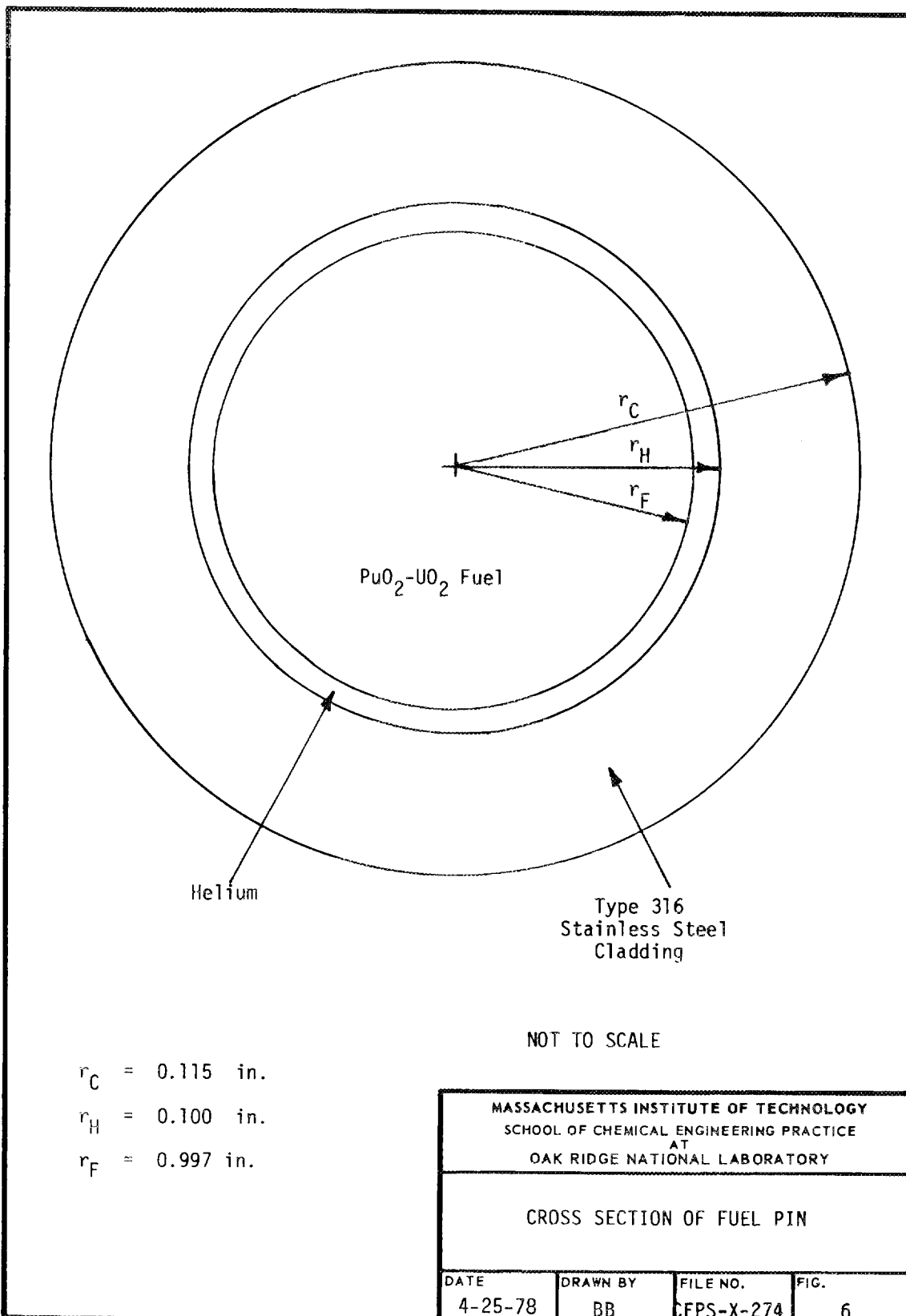
at $r = 0$,

$$\frac{dT}{dr} = 0 \quad (21)$$

at $r = r_F$

$$T(r = r_F^-) = T(r = r_F^+) \quad (22)$$

$$k_F \left. \frac{dT}{dr} \right|_{r=r_F^-} = k_H \left. \frac{dT}{dr} \right|_{r=r_F^+} \quad (23)$$



at $r = r_H^-$,

$$T(r = r_H^-) = T(r = r_H^+) \quad (24)$$

$$K_H \frac{dT}{dr} \Big|_{r=r_H^-} = K_C \frac{dT}{dr} \Big|_{r=r_H^+} \quad (25)$$

at $r = r_C$,

$$K_C \frac{dT}{dr} + h(T - T_{Na}) = 0 \quad (26)$$

The heat transfer coefficient in Eq. (26) includes both convective and radiative effects.

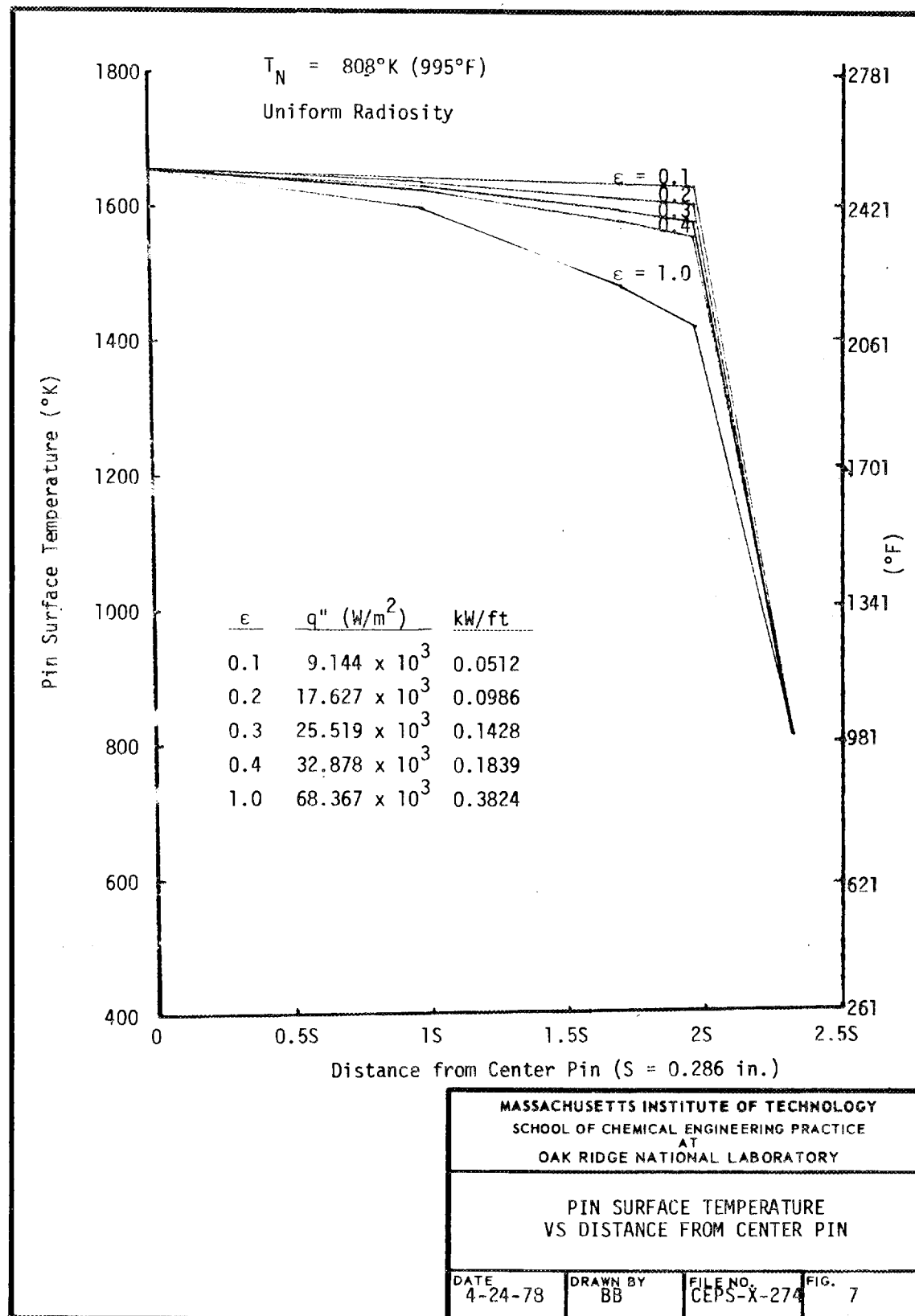
4. RESULTS AND DISCUSSION

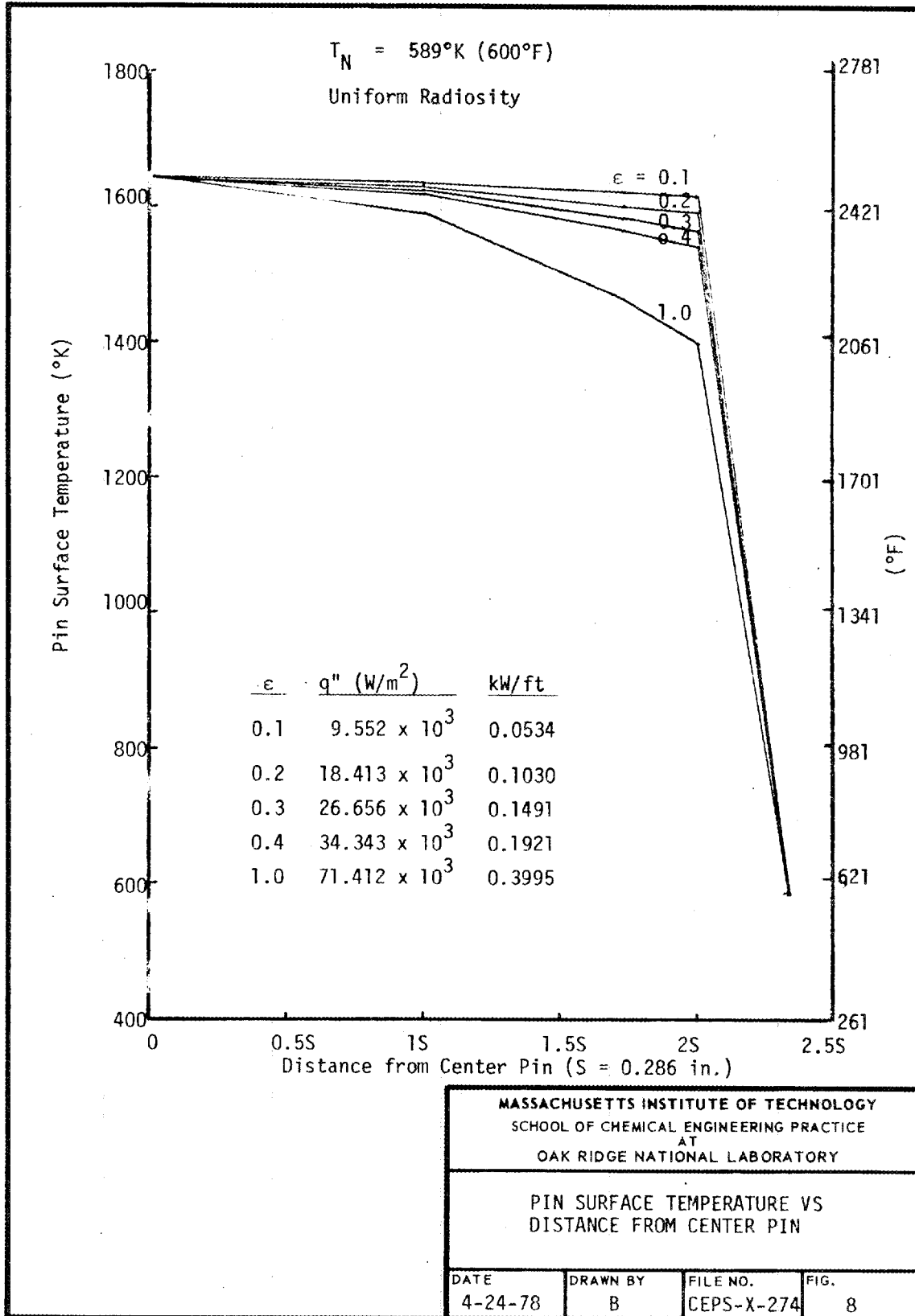
4.1 Pin Surface Temperature Distributions

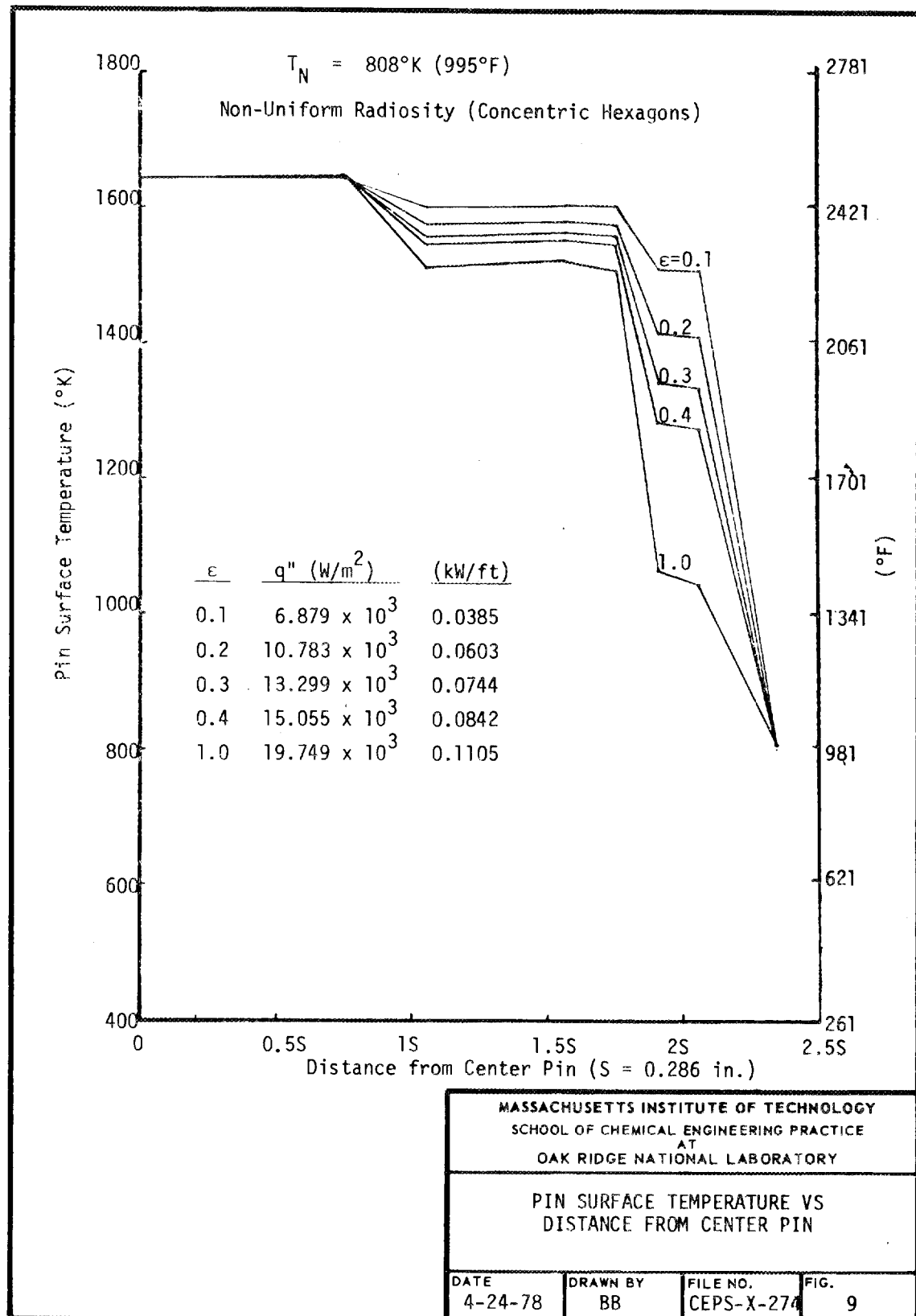
Pin surface temperature distributions were calculated for the three radiosity configurations for four duct-wall temperatures and for a range of emissivities. These results are tabulated in Tables 3 through 5 in Appendix 8.1. Pin surface temperature distributions for the two extreme duct-wall temperatures of 808 and 589 K are plotted in Figs. 7 through 12. In these figures, distance from the center pin is defined as the length from the center of the bundle to the centroid of the pin section. The maximum allowable uniform pin power, q'' , is also tabulated for various values of emissivity on each figure.

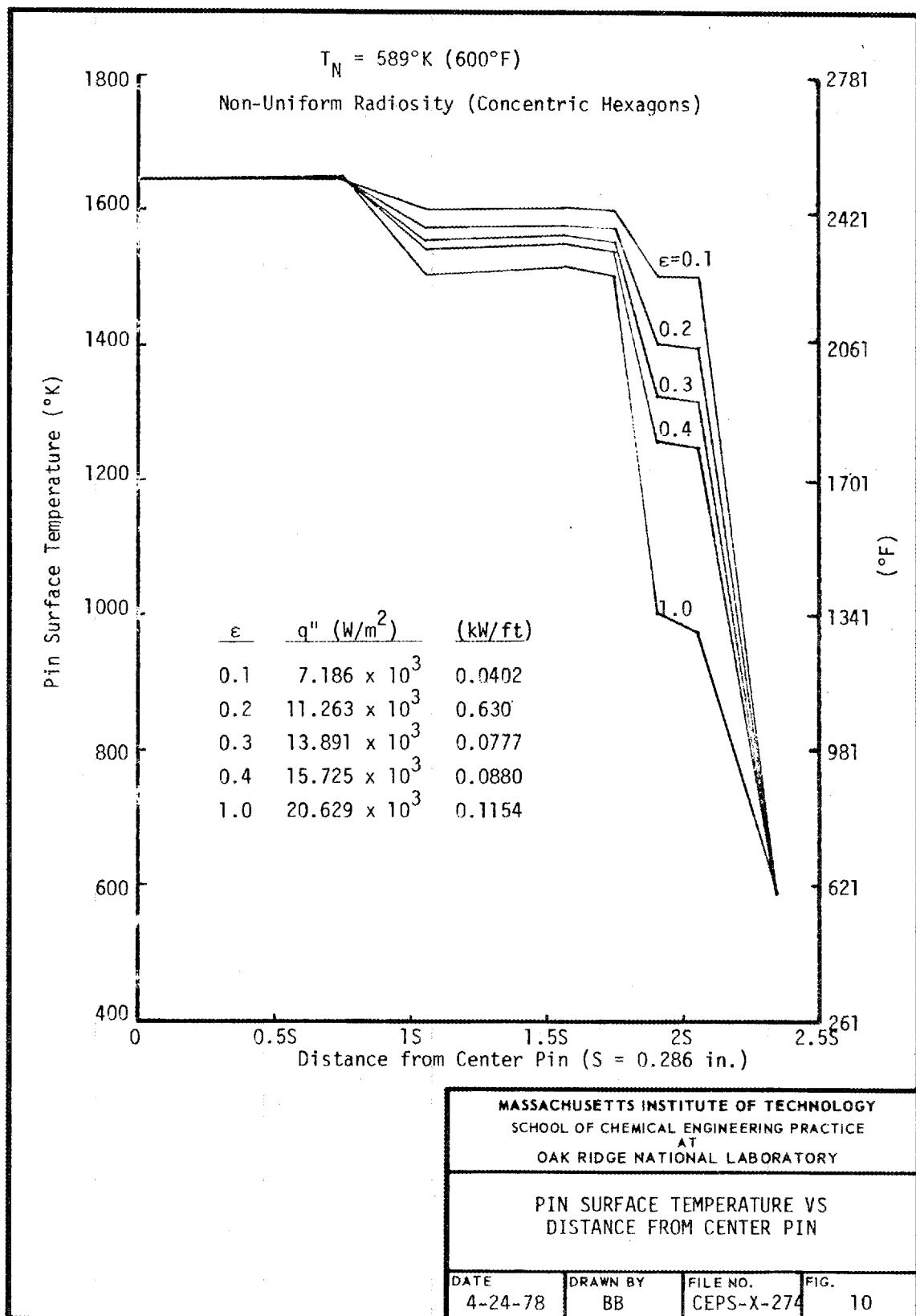
Comparing Figs. 7 and 8, 9 and 10, and 11 and 12, it is seen that the temperature distribution and the maximum allowable uniform pin power generation rate do not vary significantly for the two duct-wall temperatures. Figure 13 shows the maximum allowable uniform pin power generation rate plotted versus duct temperature for various emissivity values. The flat portions of Fig. 13 indicate that for a wide range of duct-wall temperatures the pin surfaces behave as if they are surrounded by an "absolute zero" environment. This can be explained by considering that the net radiation exchange between two infinite, parallel black surfaces at temperatures T_1 and T_2 is given by

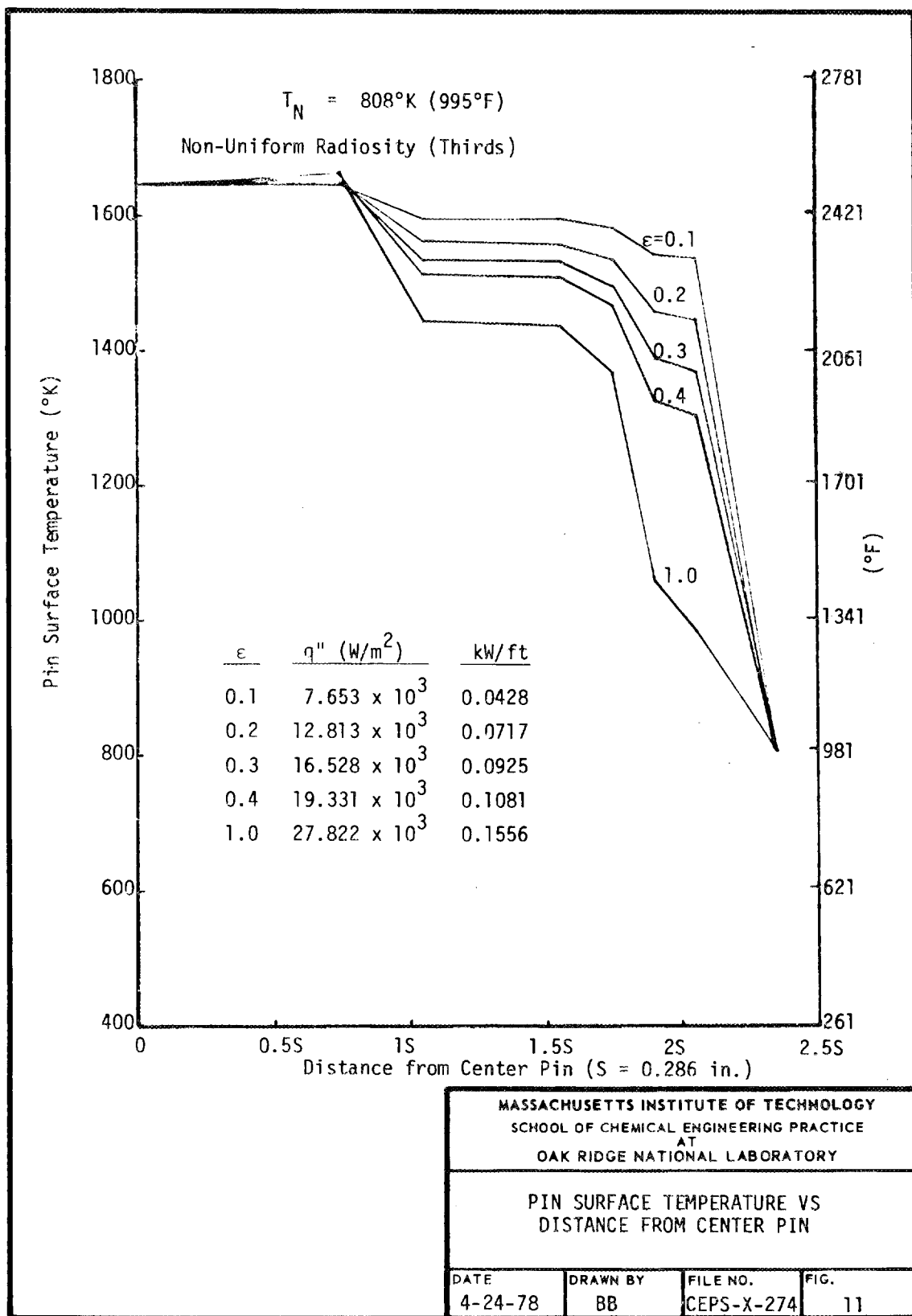
$$\text{net radiation} = \sigma(T_1^4 - T_2^4) \sim \sigma T_1^4, \text{ for } T_2 \leq 0.5 T_1 \quad (27)$$

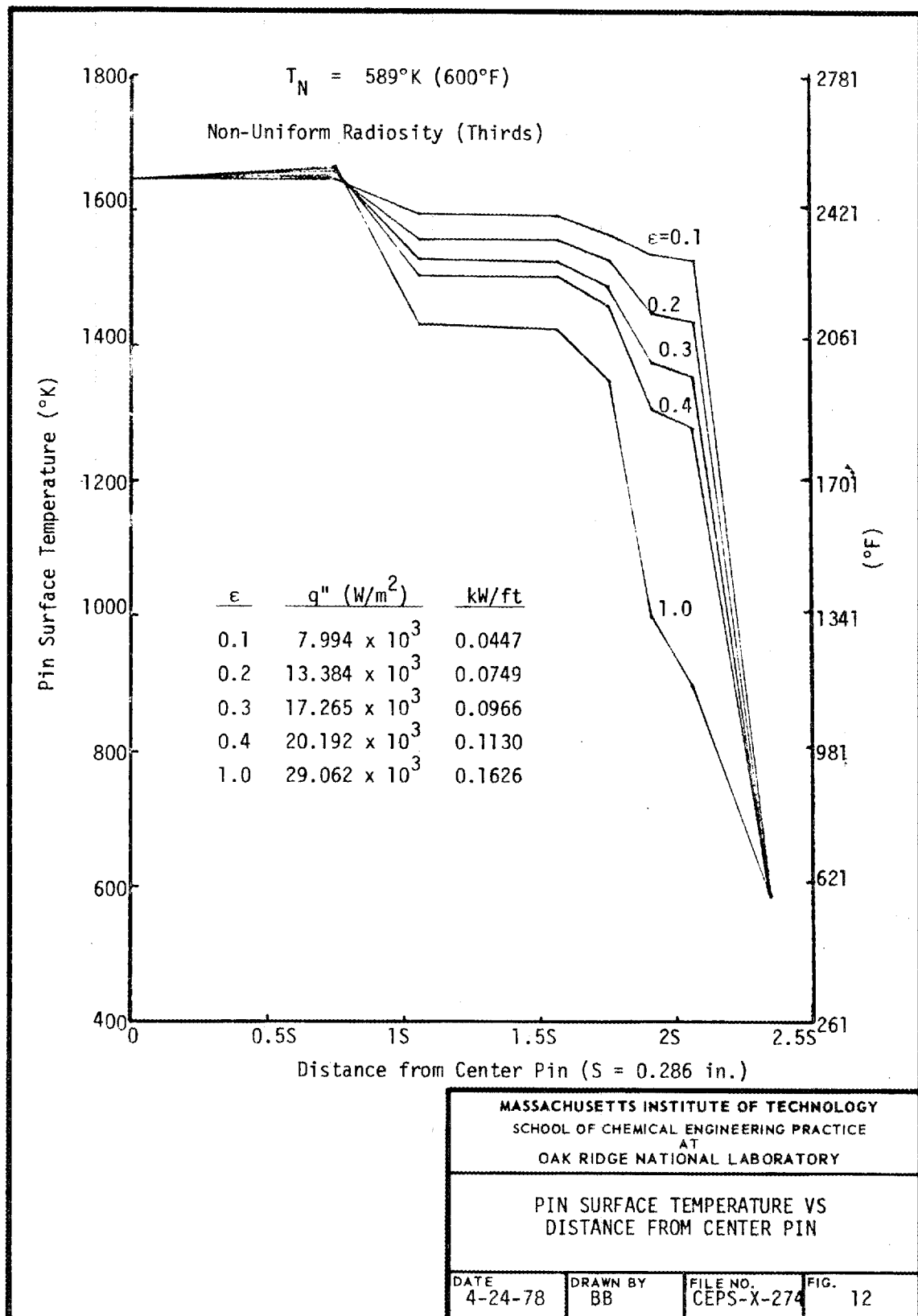


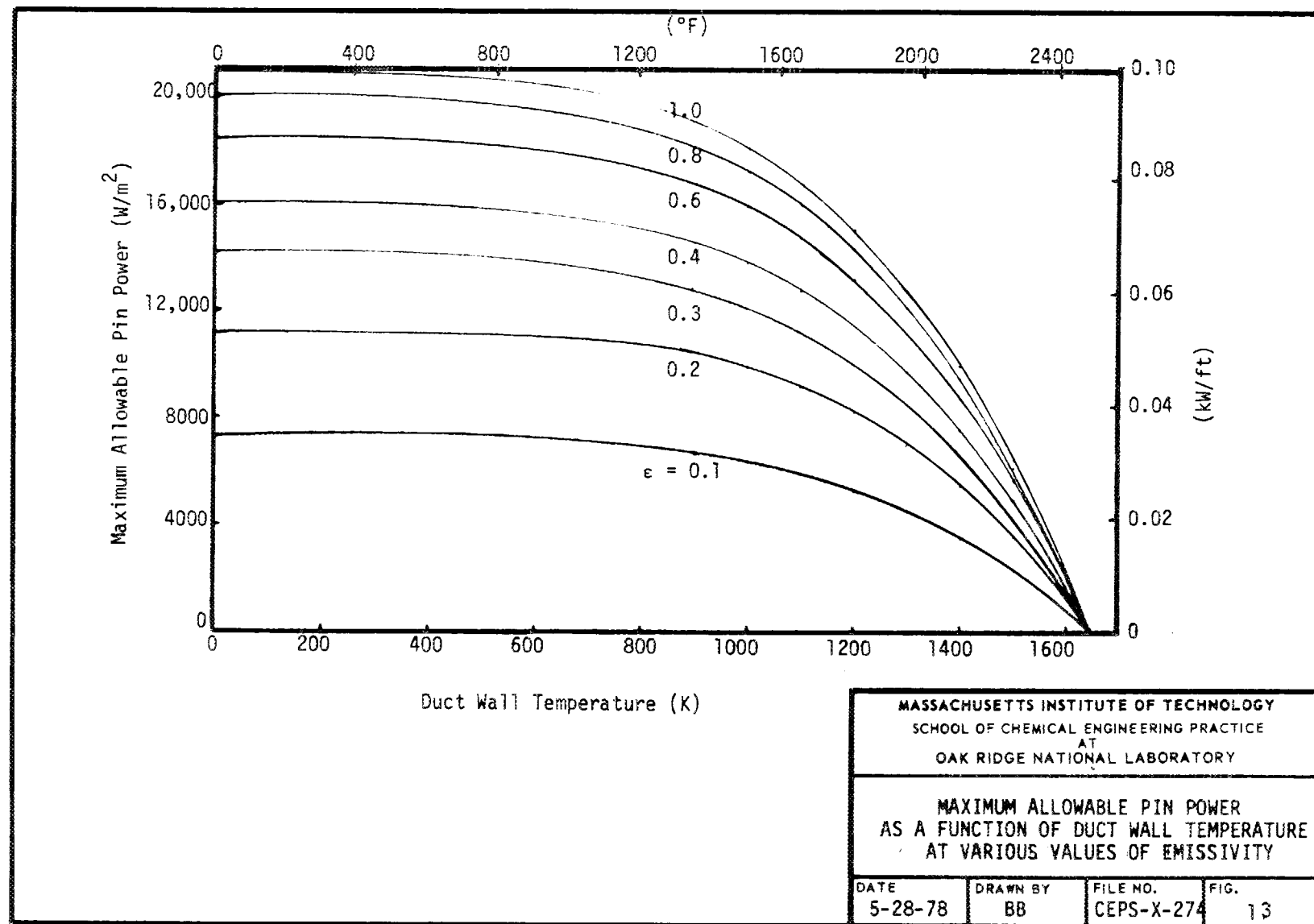












A comparison of Figs. 7 and 8 with Figs. 9 through 12 shows that non-uniform radiosity gives a smoother temperature change from pin to pin near the wall. Also, the temperature difference between the coldest pin surface and the duct wall is the least for the nonuniform cases. The range of q'' for uniform radiosity is also much higher than that for nonuniform radiosity. Physically, the assumption of uniform radiosity around the pin surface is a poor one (except for the center pin) as can be explained using Eq. (2). If B_i is uniform, H_i must also be uniform so the pin can be uniformly irradiated around its surface. This is clearly inaccurate since all the pins except the one at the center are surrounded by surfaces at different temperatures.

4.2 Comparison of Radiative Heat Transfer with Other Modes of Heat Transfer

Figures 14 and 15 show q'' as a function of ΔT for the two extreme wall temperatures, where ΔT is the temperature difference between the pin surface and the duct wall. As the emissivity decreases from a perfect black body to a gray body for a given q'' , the pin temperature increases. Based on an emissivity of 0.3 (which realistically describes the surfaces of the fuel element cladding), the capability for heat removal by radiation lies between 2000 and 20,000 W/m².

In a hypothetical core-disruptive accident, the boiling off of sodium liquid will be followed by simultaneous free and forced convection of sodium vapor with radiation because sodium vapor is transparent to radiation (13). Therefore radiative heat transfer behaves as an add-on cooling mechanism.

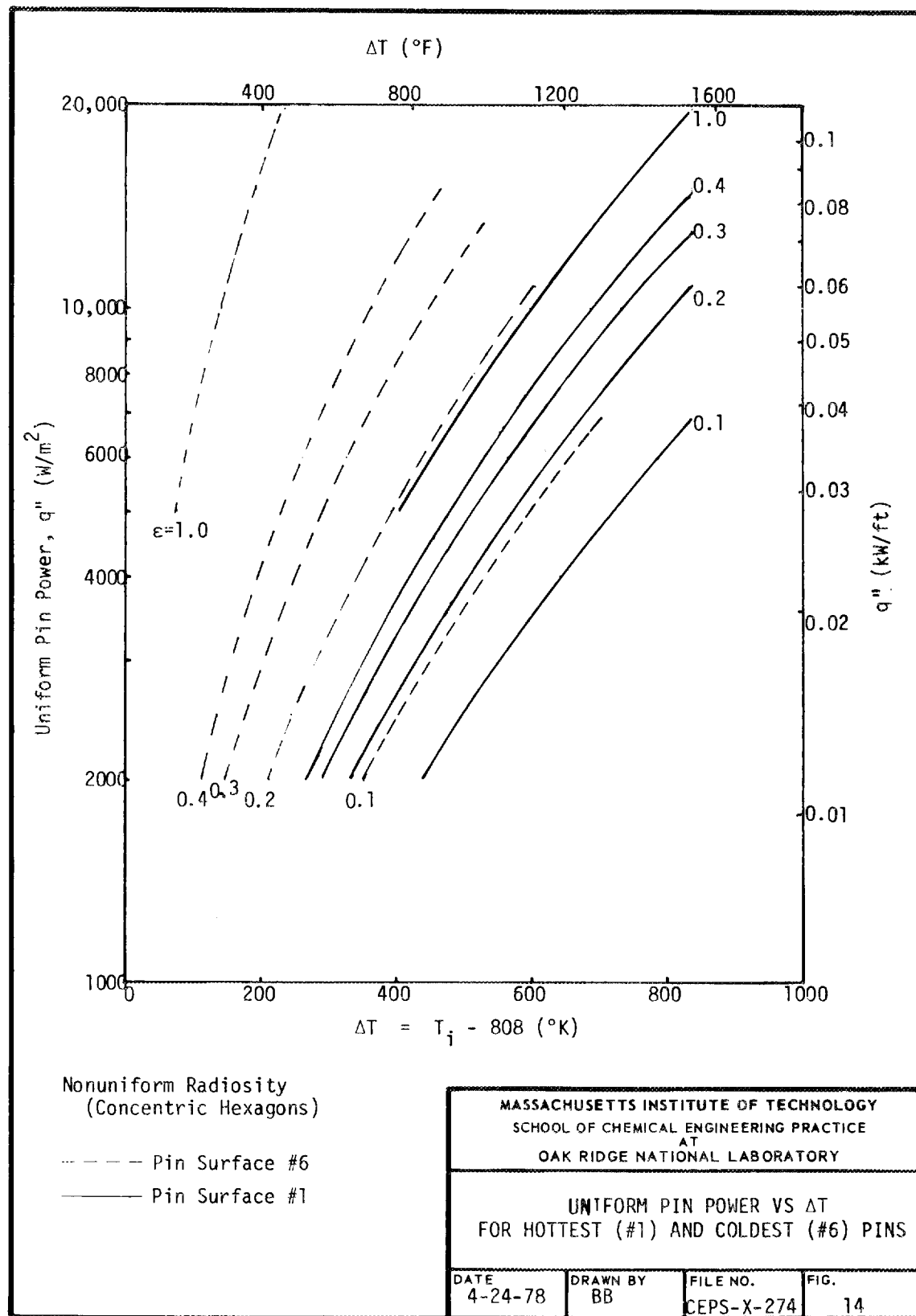
Figure 16 is a combined graph of various modes of heat transfer. Free convection (sodium vapor) heat transfer ranges from 2000 to 4000 W/m² (0.011 to 0.022 kW/ft) for Reynolds' numbers ranging from 2000 to 10,000. Forced convection (sodium vapor) heat transfer ranges from 20,000 to 400,000 W/m² (0.112 and 2.24 kW/ft). Flow-boiling heat transfer is naturally larger, ranging from 100,000 to 80,000,000 W/m² (0.56 to 447.5 kW/ft). Radiative heat transfer falls between that of free and forced convection.

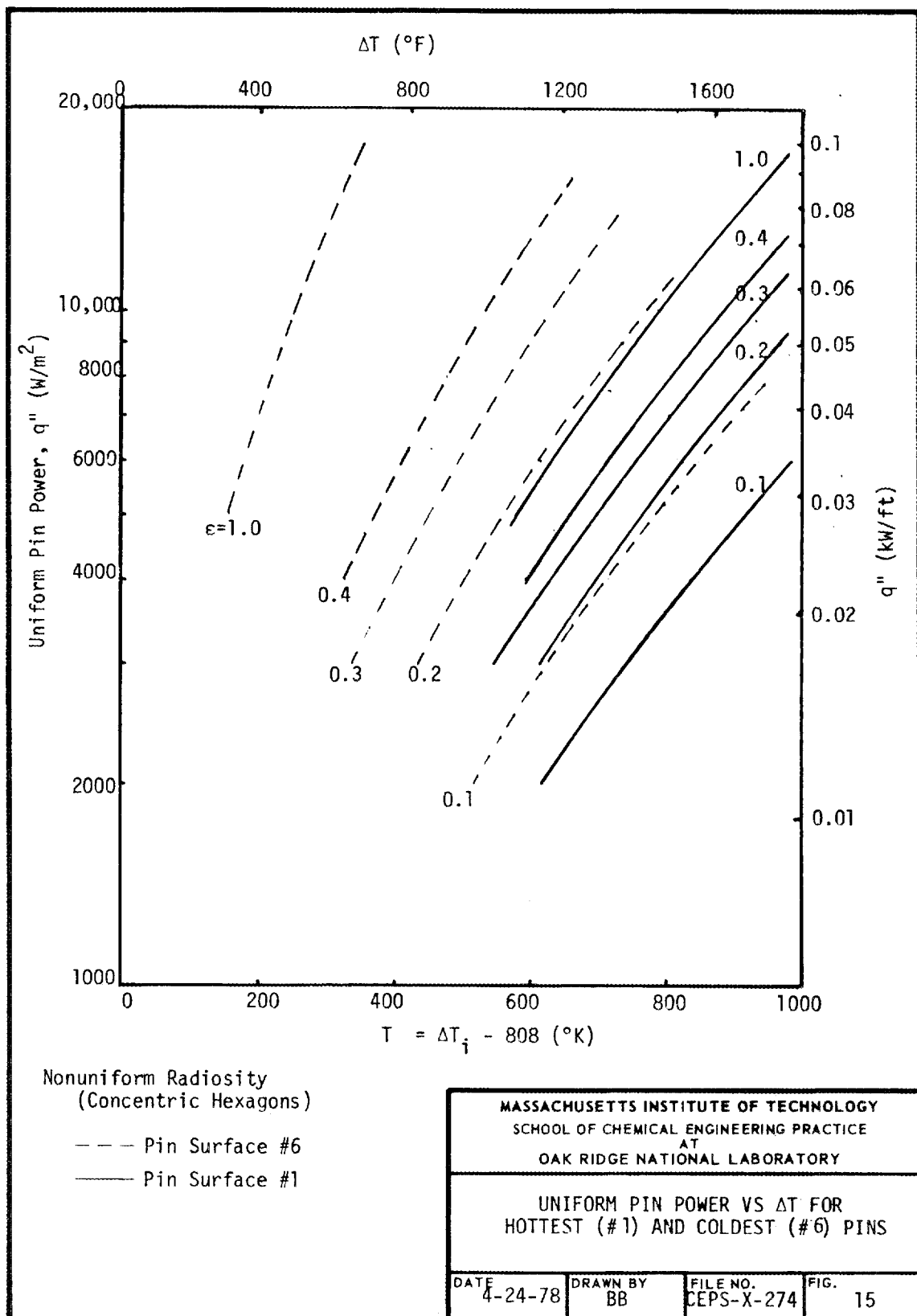
4.3 Radial Temperature Distribution of the Center Pin

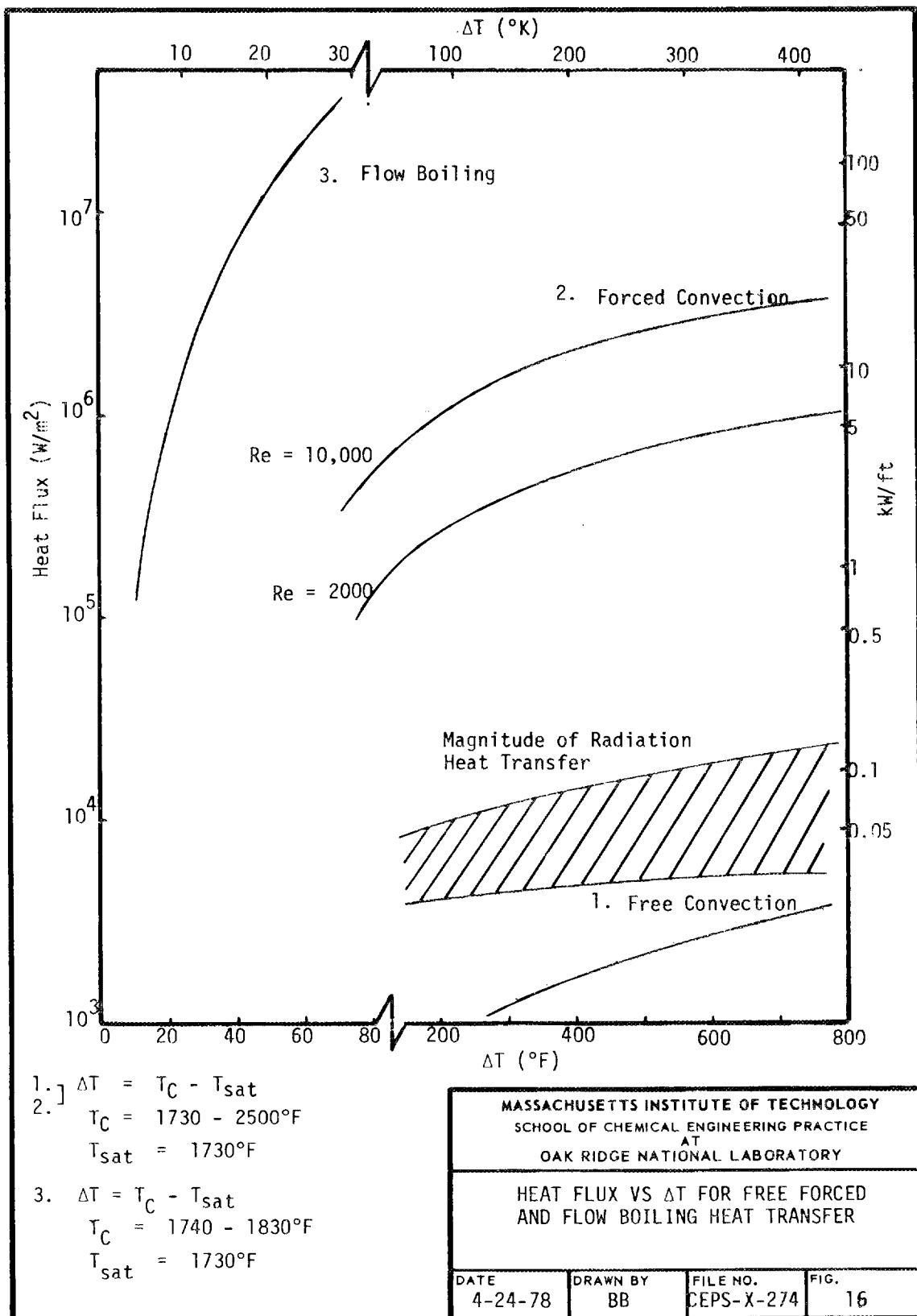
The temperature profile in the fuel element (see Fig. 6) is given by:

$$T - T_{Na} = \frac{Q_V r_F^2}{4K_F} \left[1 - \left(\frac{r}{r_F} \right)^2 + 2 \frac{K_F}{K_H} \ln \left(\frac{r_H}{r_F} \right) + 2 \frac{K_F}{K_C} \ln \left(\frac{r_C}{r_H} \right) + \frac{2K_F}{r_C h} \right] \quad (28)$$

For the helium gap (neglecting convection):







$$T - T_{Na} = \frac{Q_V r_F^2}{2K_H} \left[\ln\left(\frac{r_H}{r}\right) + \frac{K_H}{K_C} \ln\left(\frac{r_C}{r_H}\right) + \frac{K_H}{r_C h} \right] \quad (29)$$

Similarly for the cladding:

$$T - T_{Na} = \frac{Q_V r_F^2}{2K_C} \left[\ln\left(\frac{r_C}{r}\right) - \frac{K_C}{r_C h} \right] \quad (30)$$

The thermal conductivities of the fuel, the 316 stainless steel, and the helium are found in Refs. (1), (16), and (20). The temperature of the fuel element at $r=0$ is given in Table 2 as a function of T_{Na} , the temperature of saturated sodium liquid, for pin powers ranging from 3.237×10^8 to 1.619×10^9 W/m² (2 to 10 kW/ft). The steady-state center temperature of the fuel exceeds its melting point of 3073 K (5072°F) (1) only at the extreme conditions of full power and sodium temperatures near 1200 K (1700°F).

Table 2. Center-Pin Centerline Temperature for Various Values of Sodium Temperature (T_{Na})* and Pin Power (Eq. 29)

Pin Power = 10^6 W/m ³ (kW/ft)									
T_{Na}		2 (344)		5 (860)		7 (1204)		10 (1720)	
°K	(°F)	°K	(°F)	°K	(°F)	°K	(°F)	°K	(°F)
734	(862)	1102	(1524)	1776	(2737)	2265	(3618)	2883	(4730)
800	(981)	1176	(1657)	1796	(2773)	2302	(3684)	2922	(4800)
1000	(1340)	1377	(2019)	2007	(3153)	2450	(3951)	3013	(4964)
1200	(1701)	1576	(2377)	2185	(3474)	2587	(4197)	3125	(5166)
1400	(2060)	1776	(2737)	2363	(3794)	2733	(4460)	3265	(5418)
1600	(2421)	1975	(3096)	2537	(4107)	2886	(4735)	3376	(5617)

*Sodium is assumed to be in the liquid state at all values of T_{Na} .

5. CONCLUSIONS

1. Radiative heat transfer in a 19-pin bundle ranges from 2000 to 20,000 W/m² (0.017 to 0.095 kW/ft). This lies between forced and free convection of sodium vapor (10^5 to 8×10^7 W/m² and 2000 to 10,000 W/m², respectively).
2. The uniform-radiosity assumption results in unrealistically high pin powers and temperature distributions that are not as gradual as those calculated by using nonuniform-radiosity assumptions.
3. For nonuniform radiosity, division of the pin bundle into three concentric hexagons gives more realistic results than does the division of each pin surface into thirds.
4. Pin surface temperature decreases with increasing emissivity.
5. The steady-state centerline temperature of the center fuel element exceeds its melting point of 3073 K (5072°F) only in the extreme steady-state conditions.

6. RECOMMENDATIONS

1. Extend this study to 217-pin bundles.
2. Investigate other divisions of pin surfaces for nonuniform radiosity calculations.
3. Examine the transient behavior of the center pin to determine whether cladding or fuel melts first after a hypothetical LMFBR accident.

7. ACKNOWLEDGMENTS

The authors thank J.T. Han for his advice and assistance during the project. We also thank M.H. Fontana for his support and encouragement.

8. APPENDIX

8.1 Additional Results

Pin surface temperatures for the three geometrical configurations studied are given in Tables 3, 4, and 5 as a function of uniform pin power generation rates and emissivities. Wall temperatures were set at 808, 732, 661, and 589 K, respectively.

Table 3. Temperature Profiles for Uniform Radiosity
(See Fig. 2)

$T_N = 808.15^\circ\text{K} = T_5$	ε	T_1 (°K)	T_2 (°K)	T_3 (°K)	T_4 (°K)	q'' (W/m ²)
0.1	1644	1637	1618	1624	9.144 $\times 10^3$	
0.2	1644	1631	1593	1604	17.627 $\times 10^3$	
0.3	1644	1625	1569	1586	25.519 $\times 10^3$	
0.4	1644	1620	1546	1569	32.878 $\times 10^3$	
0.5	1644	1614	1522	1551	39.758 $\times 10^3$	
0.6	1644	1609	1500	1535	46.203 $\times 10^3$	
0.7	1644	1605	1477	1518	52.253 $\times 10^3$	
0.8	1644	1601	1455	1503	57.942 $\times 10^3$	
0.9	1644	1596	1438	1487	63.305 $\times 10^3$	
1.0	1644	1592	1412	1472	68.367 $\times 10^3$	
$T_N = 732.04^\circ\text{K} = T_5$						
0.1	1644	1637	1617	1624	9.329 $\times 10^3$	
0.2	1644	1631	1592	1604	17.984 $\times 10^3$	
0.3	1644	1625	1578	1585	26.036 $\times 10^3$	
0.4	1644	1619	1543	1567	33.544 $\times 10^3$	

Table 3 (Continued)

<u>ϵ</u>	<u>T_1</u> (°K)	<u>T_2</u> (°K)	<u>T_3</u> (°K)	<u>T_4</u> (°K)	<u>q''</u> (W/m ²)
0.5	1644	1614	1520	1549	40.563×10^3
0.6	1644	1609	1496	1532	47.138×10^3
0.7	1644	1604	1473	1515	53.311×10^3
0.8	1644	1600	1451	1499	59.117×10^3
0.9	1644	1595	1428	1484	64.589×10^3
1.0	1644	1591	1406	1468	69.753×10^3
<u>$T_N = 660.93^\circ K = T_5$</u>					
0.1	1644	1637	1617	1623	9.458×10^3
0.2	1644	1631	1592	1603	18.232×10^3
0.3	1644	1625	1566	1584	26.393×10^3
0.4	1644	1619	1542	1566	34.005×10^3
0.5	1644	1614	1518	1548	41.120×10^3
0.6	1644	1609	1494	1530	47.786×10^3
0.7	1644	1604	1470	1513	54.044×10^3
0.8	1644	1599	1447	1497	59.929×10^3
0.9	1644	1595	1425	1481	65.475×10^3
1.0	1644	1591	1402	1465	70.711×10^3
<u>$T_N = 588.71^\circ K = T_5$</u>					
0.1	1644	1637	1617	1623	9.552×10^3
0.2	1644	1631	1591	1603	18.413×10^3
0.3	1644	1625	1566	1584	26.656×10^3
0.4	1644	1619	1541	1565	34.343×10^3
0.5	1644	1613	1516	1546	41.529×10^3

Table 3 (Continued)

ε	(°K)	(°K)	(°K)	(°K)	q'' (W/m ²)
0.6	1644	1608	1492	1529	48.261×10^3
0.7	1644	1603	1468	1512	54.581×10^3
0.8	1644	1599	1445	1495	60.525×10^3
0.9	1644	1594	1422	1479	66.127×10^3
1.0	1644	1590	1399	1463	71.412×10^3

Table 4. Temperature Profiles for Non-Uniform Radiosity (Hexagons)
(see Fig. 3)

$$T_N = 808.15^\circ\text{K} = T_8$$

ε	T_1 (°K)	T_2 (°K)	T_3 (°K)	T_4 (°K)	T_5 (°K)	T_6 (°K)	T_7 (°K)	q° (W/m ²)
0.1	1644	1646	1601	1601	1604	1508	1510	6.879×10^3
0.2	1644	1647	1576	1575	1581	1410	1415	10.783×10^3
0.3	1644	1648	1559	1557	1565	1335	1342	13.299×10^3
0.4	1644	1648	1547	1545	1554	1274	1283	15.055×10^3
0.5	1644	1649	1537	1535	1547	1223	1236	16.350×10^3
0.6	1644	1649	1530	1528	1539	1178	1190	17.345×10^3
0.7	1644	1649	1524	1522	1534	1139	1153	18.134×10^3
0.8	1644	1649	1519	1517	1529	1103	1120	18.774×10^3
0.9	1644	1649	1515	1512	1526	1072	1090	19.303×10^3
1.0	1644	1649	1512	1509	1522	1043	1063	19.749×10^3

Table 4 (Continued)

$T_N = 732.04 = T_8$								
ϵ	T_1 (°K)	T_2 (°K)	T_3 (°K)	T_4 (°K)	T_5 (°K)	T_6 (°K)	T_7 (°K)	q'' (W/m ²)
0.1	1644	1646	1601	1600	1664	1505	1507	7.019×10^3
0.2	1644	1647	1575	1573	1580	1405	1409	11.001×10^3
0.3	1644	1648	1557	1555	1564	1327	1334	13.568×10^3
0.4	1644	1648	1544	1543	1552	1263	1272	15.360×10^3
0.5	1644	1649	1535	1533	1543	1209	1220	16.682×10^3
0.6	1644	1649	1527	1525	1537	1161	1174	17.697×10^3
0.7	1644	1649	1521	1519	1531	1119	1134	18.501×10^3
0.8	1644	1649	1517	1514	1527	1081	1099	19.154×10^3
0.9	1644	1650	1512	1510	1523	1047	1067	19.695×10^3
1.0	1644	1650	1509	1506	1520	1014	1037	20.149×10^3
$T_N = 660.93^{\circ}\text{K} = T_8$								
0.1	1644	1646	1600	1599	1603	1503	1505	7.115×10^3
0.2	1644	1647	1574	1572	1579	1401	1405	11.153×10^3
0.3	1644	1648	1556	1554	1563	1321	1328	13.755×10^3
0.4	1644	1648	1543	1541	1551	1255	1264	15.571×10^3
0.5	1644	1649	1533	1531	1542	1198	1210	16.911×10^3
0.6	1644	1649	1526	1523	1535	1149	1163	17.940×10^3
0.7	1644	1649	1519	1517	1529	1105	1121	18.755×10^3
0.8	1644	1649	1515	1512	1525	1065	1083	19.417×10^3
0.9	1644	1649	1510	1507	1521	1028	1049	19.965×10^3
1.0	1644	1650	1507	1504	1518	993	1017	20.426×10^3

Table 4 (Continued)

 $T_N = 588.71^\circ K = T_8$

ϵ	T_1 (°K)	T_2 (°K)	T_3 (°K)	T_4 (°K)	T_5 (°K)	T_6 (°K)	T_7 (°K)	q'' (W/m ²)
0.1	1644	1646	1600	1599	1603	1501	1503	7.186×10^3
0.2	1644	1647	1573	1572	1578	1397	1402	11.263×10^3
0.3	1644	1648	1555	1553	1562	1316	1323	13.891×10^3
0.4	1644	1649	1542	1539	1550	1249	1258	15.725×10^3
0.5	1644	1649	1532	1530	1541	1191	1203	17.079×10^3
0.6	1644	1649	1524	1522	1534	1140	1154	18.118×10^3
0.7	1644	1649	1518	1516	1528	1094	1111	18.941×10^3
0.8	1644	1649	1513	1510	1524	1052	1072	19.610×10^3
0.9	1644	1650	1509	1506	1520	1013	1036	20.163×10^3
1.0	1644	1650	1505	1502	1516	977	1002	20.629×10^3

Table 5. Temperature Profiles for Non-Uniform Radiosity (Thirds)
(see Fig. 4) $T_N = 808.15 = T_8$

ϵ	T_1 (°K)	T_2 (°K)	T_3 (°K)	T_4 (°K)	T_5 (°K)	T_6 (°K)	T_7 (°K)	q'' (W/m ²)
0.1	1644	1647	1596	1581	1594	1535	1541	7.65×10^3
0.2	1644	1649	1561	1534	1558	1446	1458	12.813×10^3
0.3	1644	1650	1535	1497	1531	1369	1388	16.528×10^3
0.4	1644	1652	1514	1468	1509	1302	1328	19.331×10^3
0.5	1644	1653	1497	1443	1491	1241	1273	21.519×10^3
0.6	1644	1653	1483	1423	1476	1185	1225	23.277×10^3
0.7	1644	1654	1471	1405	1464	1132	1180	24.720×10^3

Table 5 (Continued)

ε	T_1 (°K)	T_2 (°K)	T_3 (°K)	T_4 (°K)	T_5 (°K)	T_6 (°K)	T_7 (°K)	(W/m^2)
0.8	1644	1654	1461	1390	1453	1081	1138	25.924×10^3
0.9	1644	1655	1452	1377	1443	1031	1098	26.945×10^3
1.0	1644	1655	1444	1365	1436	982	1060	27.822×10^3
$T_N = 732.04 = T_8$								
0.1	1644	1647	1595	1580	1593	1532	1539	7.807×10^3
0.2	1644	1649	1560	1532	1556	1441	1454	13.073×10^3
0.3	1644	1651	1532	1494	1528	1362	1381	16.863×10^3
0.4	1644	1652	1511	1464	1506	1292	1319	19.722×10^3
0.5	1644	1653	1493	1438	1487	1228	1262	21.956×10^3
0.6	1644	1653	1479	1417	1472	1168	1210	23.749×10^3
0.7	1644	1654	1468	1399	1459	1111	1163	25.220×10^3
0.8	1644	1654	1456	1383	1448	1056	1118	26.450×10^3
0.9	1644	1655	1447	1370	1439	1001	1075	27.491×10^3
1.0	1644	1655	1439	1357	1430	946	1034	28.386×10^3
$T_N = 660.93 = T_8$								
0.1	1644	1647	1595	1579	1593	1531	1537	7.9×10^3
0.2	1644	1649	1558	1530	1555	1437	1450	13.252×10^3
0.3	1644	1651	1531	1492	1526	1357	1377	17.094×10^3
0.4	1644	1652	1509	1461	1503	1285	1312	19.993×10^3
0.5	1644	1653	1491	1435	1485	1219	1254	22.258×10^3
0.6	1644	1654	1476	1413	1469	1157	1201	24.076×10^3
0.7	1644	1654	1464	1395	1456	1097	1151	25.567×10^3
0.8	1644	1655	1453	1379	1445	1038	1103	26.812×10^3

Table 5 (Continued)

ε	T_1 (°K)	T_2 (°K)	T_3 (°K)	T_4 (°K)	T_5 (°K)	T_6 (°K)	T_7 (K°)	q'' (W/m ²)
0.9	1644	1655	1443	1365	1435	979	1058	27.869×10^3
1.0	1644	1655	1436	1352	1427	918	1014	28.775×10^3
$T_N = 588.71 = T_8$								
0.1	1644	1647	1594	1578	1592	1529	1536	7.994×10^3
0.2	1644	1649	1558	1529	1554	1435	1448	13.384×10^3
0.3	1644	1651	1529	1490	1525	1353	1373	17.265×10^3
0.4	1644	1652	1507	1458	1502	1279	1307	20.192×10^3
0.5	1644	1653	1489	1432	1483	1212	1248	22.479×10^3
0.6	1644	1654	1474	1410	1467	1147	1193	24.314×10^3
0.7	1644	1654	1462	1392	1454	1086	1142	25.821×10^3
0.8	1644	1655	1451	1375	1442	1024	1093	27.079×10^3
0.9	1644	1655	1442	1361	1432	962	1046	28.146×10^3
1.0	1644	1655	1433	1348	1424	897	999	29.062×10^3

8.2 View Factors

View factors for the three sets of surfaces examined are given in Tables 6, 7, and 8 with the following set of notations:

- U The corresponding view factor is explicitly calculated for uniform-radiosity.
- T The corresponding view factor is explicitly calculated for nonuniform-radiosity (thirds).
- H The corresponding view factor is explicitly calculated for nonuniform-radiosity (concentric hexagons).

Table 6. View Factors for Uniform Radiosity
(Fig. 2)

F _{1j}				F _{2j}				F _{3j}				F _{4j}				F _{5j}			
View Factor	Value	No.	Note	View Factor	Value	No.	Note	View Factor	Value	No.	Note	View Factor	Value	No.	Note	View Factor	Value	No.	Note
F ₁₂	0.136849	6	U	F ₂₁	0.136849	1	REC	F ₃₂	0.136849	1	REC	F ₄₁	0.28898	1	REC	F ₅₁	0.000902	1	REC
F ₁₄	0.028898	6	U	F _{22a}	0.136849	2	F _{12,U}	F _{32a}	0.028898	2	REC	F ₄₂	0.136849	2	REC	F ₅₂	0.010108	6	REC
F ₁₅	0.005518	1	REM	F _{22b}	0.028892	2	F _{14,U}	F _{32b}	0.000361	2	REC	F _{42b}	0.000361	2	REC	F ₅₃	0.086608	6	REC
				F ₂₃	0.136849	1	F _{12,U}	F ₃₄	0.136849	2	F _{12,U}	F ₄₃	0.136849	2	REC	F ₅₄	0.059528	6	REC
				F _{23a}	0.028898	2	F _{14,U}	F _{34b}	0.000361	2	F _{24c,U}	F _{43a}	0.000361	2	REC	F ₅₅	0.061634	1	REM
				F _{23b}	0.000361	2	F _{24c,U}	F _{34c}	0.000056	2	U	F _{43b}	0.000056	2	REC				
				F ₂₄	0.136849	2	F _{12,U}	F ₃₅	0.530101	1	REM	F _{44a}	0.028898	2	F _{14a,U}				
				F _{24c}	0.000361	2	U					F ₄₅	0.364354	1	REM				
				F ₂₅	0.061870	1	REM												

Table 7. View Factors for Non-Uniform Radiosity (Hexagons)
(see Fig. 3)

Table 8. View Factors for Non-Uniform Radiosity (Thirds)
 (see Fig. 4)

$fF_{ij,U}$ The corresponding view factor is a fraction f of F_{ij} from uniform radiosity. Similarly for $fF_{ij,T}$ and $fF_{ij,H}$

REC The corresponding view factor is calculated by reciprocity relationship:

$$F_{ji} = \frac{A_i}{A_j} F_{ij}$$

where F_{ij} has been previously calculated

REM The corresponding view factor is calculated as a remainder:

$$F_{IN} = 1 - \sum_{j=1}^{N-1} F_{1j}$$

8.3 Computer Program

The following computer program generates temperature distributions for a given set of uniform power generation rate and emissivity with the center pin temperature kept below 1644 K:

```

02      IMPLICIT REAL*8 (A-H,O-Z)
03      DIMENSION C(8,8), G(8), T(8), F(8), B(8), E(8,8), H(8), CHECK(8)
04      READ 1,N
05      1 FORMAT (I2)
06      DO 2 I=1,N
07      2 READ 3,(F(I,J),J=1,N)
08      READ 4,(Q(I), I=1,N)
09      READ 3,(T(I), I=1,N)
10      READ 5,EP
11      READ 3,TM
12      3 FORMAT (8F10.6)
13      4 FORMAT (8E10.3)
14      5 FORMAT (2F6.3)
15      K=N-1
16      QQ=Q(1)
17      8 DO 10 I=1,N
18      DO 9 J=1,N
19      9 C(I,J)=0.0
20      CHECK(I)=0.0
21      H(I)=0.0
22      P(I)=0.0
23      10 B(I)=0.0
24      DO 11 I=1,K
25      DO 11 J=1,N
26      11 C(I,J)=-F(I,J)
27      DO 12 I=1,K
28      12 C(I,I)=1.0-F(I,I)
29      DO 15 J=1,K
30      15 C(N,J)=-(1.0-EP)*F(N,J)
31      C(N,N)=1.0-(1.0-EP)*F(N,N)
32      Q(N)=(EP*5.669E-8)*T(N)**4
33      DO 20 I=1,N

```

```

34      20 P(I)=Q(I)
35      CALL DMATEQ(C,F,N,1,8)
36      DO 30 I=1,N
37      30 B(I)=P(I)
38      DO 70 I=1,N
39      DO 70 J=1,N
40      H(I)=H(I)+B(J)*F(I,J)
41      70 CHECK(I)=B(I)-H(I)
42      CHECK(N)=B(N)-(1.0-EP)*H(N)
43      DO 80 I=1,K
44      80 T(I)=((Q(I)/EP)+H(I))/5.669E-8)**.25
45      DO 90 I=1,N
46      90 PRINT 100,I,Q(I),E(I),T(I),H(I),CHECK(I)
47      100 FORMAT (I2,5(3X,E12.6))
48      PRINT 220,EP
49      220 FORMAT(5X,E12.6////////)
50      IF(T(1) .GT. TM) GO TO 225
51      Q(1)=Q(1)+QQ
52      DO 221 I=2,K
53      221 Q(I)=Q(1)
54      GO TO 8
55      225 IF (EP.GT. 0.9) GO TO 230
56      EP =EP+0.1
57      DO 226 I=1,K
58      226 Q(I)=QQ
59      GO TO 8
60      230 STOP
61
62      END
63

```

8.4 Sample Heat Transfer Calculations

8.4.1 Free Convection of Sodium Vapor (10, 14)

For vertical laminar flow ($Gr_x < 10^9$), the local Nusselt number is

$$Nu_x = 0.508 \Pr^{1/2} (0.952 + \Pr)^{-1/4} (Gr_x)^{1/4}$$

$$Gr_x = \frac{\rho \beta g x^3 \Delta T}{\mu^2}$$

Thus the length-averaged Nusselt number is

$$\overline{Nu} = \int_0^L \frac{Nu_x}{x} dx$$

characteristic pin length, L = 3 ft

Obtaining the length-averaged heat transfer coefficient and integrating gives:

$$\bar{h} = 0.515 K \Pr^{1/2} (0.952 + \Pr)^{-1/4} \left(\frac{\rho^2 \beta g \Delta T}{\mu^2} \right)^{1/4} \quad (31)$$

For $T_{Na} = 1730^{\circ}\text{F}$, $T_c = 2500^{\circ}\text{F}$, $T_{film} = T_{Na} + [(T_c - T_{Na})/2] = 2115^{\circ}\text{F}$, $\beta = 1/(2115 + 460) = 4.73 \times 10^{-4} \text{ }^{\circ}\text{R}^{-1}$, $\Delta T = 770^{\circ}\text{F}$, $k = 0.485 \text{ Btu/hr-ft-}^{\circ}\text{F}$, $\Pr = 0.765$, $\mu = 0.05156 \text{ lb/hr-ft}$, $\rho = 0.0251 \text{ lb/ft}^3$, and $g = 4.1472 \times 10^8 \text{ ft/hr}^2$,

$$Gr_x = 9.66 \times 10^8$$

$$\bar{h} = 14.76 \text{ Btu/hr-ft}^2 \text{-}^{\circ}\text{F}$$

Thus,

$$\frac{Q}{A} = h \Delta T = 11,365 \text{ Btu/hr-ft}^2 = 35,829 \text{ W/m}^2 = 2 \times 10^{-1} \text{ kW/ft}$$

8.4.2 Forced Convection of Sodium Vapor (8, 10, 14)

If it is assumed that $Re = 10,000$ and if the vapor properties of the previous section are used:

$$Nu = 0.023 Re^{0.8} \Pr^{0.4} = 32.75 \quad (16)$$

hydraulic diameter, $D_H = 0.00995 \text{ ft}$

$$h = \frac{Nu K}{D_H} = 1596.4 \text{ Btu/hr-ft}^2 \text{-}^{\circ}\text{F}$$

Thus,

$$\frac{Q}{A} = h \Delta T = 1,229,228 \text{ Btu/hr-ft}^2 = 3,875,118 \text{ W/m}^2 = 21.7 \text{ kW/ft}$$

8.4.3 Flow-Boiling Heat Transfer of Liquid Sodium

Labuntsov's equation (9) for flow-boiling heat transfer is:

$$\frac{\frac{Q}{A} C_{p\ell} \rho \sigma T_{sat}}{(T_c - t_{sat}) k_\ell \lambda^2 \rho^2 J} = 0.125 \left[\frac{\frac{Q}{A} C_{p\ell} \rho \sigma T_{sat}}{\lambda^3 \rho^3 v_\ell J} \right]^{2/3} (Pr_\ell)^{2/3}$$

where:

$$Pr_\ell = \frac{C_{p\ell} \mu_\ell}{k_\ell}$$

Substituting $t_{sat} = 1730^\circ F$ (boiling point of sodium), T_c = cladding temperature ($^\circ F$), $T_{sat} = 2190^\circ R$, $C_{p\ell} = 0.3107 \text{ Btu/lb}_m \text{-}^\circ R$, $\rho_\ell = 45.265 \text{ lb}_m/\text{ft}^3$, $\sigma = 0.007698 \text{ lb}_f/\text{ft}$, $k_\ell = 28.07 \text{ Btu/hr-ft-}^\circ R$, $\lambda = 1641.65 \text{ Btu/lb}_m$, $\rho = 0.0275 \text{ lb}_m/\text{ft}^3$, $\mu_\ell = 0.3601 \text{ lb}_m/\text{ft-hr}$, $v_\ell = 0.00796 \text{ ft}^2/\text{hr}$, $J = 778.2 \text{ ft-lb}_f/\text{Btu}$, and $Pr_\ell = 0.003986$ gives

$$\frac{Q}{A} = [(3.274)(T_c - 1730)]^3$$

Q/A is obtained by varying T_c such that the temperature difference between cladding and liquid sodium is less than $100^\circ F$. For $T_c = 1740^\circ F$ ($10^\circ F$ difference):

$$\frac{Q}{A} = 35,094 \text{ Btu/hr-ft}^2 = 110,634 \text{ W/m}^2 = 0.62 \text{ kW/ft}$$

8.5 Nomenclature

- A_i surface area of i , m^2
- B_i radiosity of surface i , W/m^2
- C_{ij} matrix of coefficients used in computer program
- C_p specific heat, $\text{Btu/lb}_m \text{-}^\circ F$
- $C_{p\ell}$ specific heat of saturated liquid, $\text{Btu/lb}_m \text{-}^\circ F$
- D_H hydraulic diameter, ft
- ϵ_P emissivity (computer program)
- F_{ij} view factor from surface i to surface j
- g acceleration due to gravity, $4.1472 \times 10^8 \text{ ft/hr}^2$
- Gr_x local Grashof number

- h heat transfer coefficient, Btu/hr-ft²-°F
 \bar{h} length-averaged heat transfer coefficient, Btu/hr-ft²-°F
 H_i irradiation to surface i , W/m²
 J constant, 778.2 ft-lb_f/Btu
 K thermal conductivity, Btu/hr-ft-°F; K_C = cladding, K_F fuel, and
 K_H helium
 L length of free convection heat transfer area, ft
 N number of unknown radiosities, B_i
 Nu Nusselt number
 Nu_b boiling Nusselt number
 Nu_x local Nusselt number
 \bar{Nu} length-averaged Nusselt number
 P_i Q_i (computer program)
 Pr Prandtl number of saturated sodium vapor
 Pr_l Prandtl number of saturated sodium liquid
 q'' pin power generation rate, W/m²
 Q_i constants used for pin power (computer program)
 Q_v volumetric heat generation, W/m³
 r radial position, in.; r_C cladding, r_F fuel, and r_H helium
 Re Reynolds number of flowing vapor
 Re_b boiling Reynolds number
 S pin pitch, in.
 T temperature, °K
 T_{Na} temperature of liquid sodium, °K
 T_{sat} temperature of saturated Na liquid as used in Labuntsov's equation, °R

t_{sat}	temperature of saturated sodium vapor at 1.7 atm, 1730°F
T_c	temperature of center pin cladding, °F
T_N	temperature of duct wall, °K
T_i	temperature of pin i, °K
V	velocity of sodium vapor, ft/sec

Greek Symbols

α	absorptivity, dimensionless
β	volumetric expansion coefficient of sodium vapor, °F ⁻¹
γ	reflectivity, dimensionless
Δ	difference operator, dimensionless
ϵ	emissivity, dimensionless
λ	latent heat of vaporization of sodium, Btu/lb _m
μ_l	viscosity of liquid sodium, lb _m /hr-ft
μ	viscosity of saturated sodium vapor, lb _m /hr-ft
ν_l	kinematic viscosity of liquid sodium, ft ² /hr
ρ_l	density of liquid sodium, lb _m /ft ³
ρ	density of saturated sodium vapor, lb _m /ft ³
σ	Stefan-Boltzman constant, $5.669 \times 10^{-8} \text{ W/m}^2 (\text{°K})^4$
σ	surface tension of sodium liquid-vapor interface, lb _m /ft

8.6 Literature References

1. Bard, F.E., B.C. Greiting, and C.M. Cox, "A Thermoelastic Material Properties Correlation for Uranium/Plutonium Mixed Oxides," HEDL-TME-74-12, Hanford Engineering Development Laboratory, Richland, Wash. (1974).
2. Carslaw, H.S., and J.C. Jaeger, "Conduction of Heat in Solids," 2nd ed., p. 191-92, Oxford University Press, London (1959).
3. Chan, S.H., et al. "Radiative Cooling in a Voided Subassembly," ANL-76-5, Argonne National Laboratory, Argonne, Ill. (1976).

4. Chan, S.H., and D. Cho, "Effect of Radiation Cooling in HCDA Radiological Consequences During Buoyancy Period," Trans. ANS, 26, 340 (1977).
5. Chan, S.H., and D. Cho, "A Calculational Method for Transient Radiation Heat Transfer in an Absorbing-Emitting Medium and Its Application to LMFBR Accident Analysis," Trans. ANS, 22, 323 (1975).
6. Chan, S.H., and D.W. Condiff, "Radiative Cooling in a Voided Sub-assembly," Trans. ANS, 22, 408 (1975).
7. Condiff, D.W., and S.H. Chan, "Studies of Radiation-Controlled Fog Formation," Trans. ANS, 22, 452 (1975).
8. Cox, R.L., "Radiative Heat Transfer in Arrays of Parallel Cylinders," ORNL-5239 (1977).
9. Dwyer, O.E., "Boiling Liquid-Metal Heat Transfer," American Nuclear Soc., Hinsdale, Ill. (1976).
10. Eckert, E.R.G., and R.M. Drake, "Heat and Mass Transfer," 2nd ed., McGraw-Hill, New York, 1959.
11. Epstein, M., and D.H. Cho, "Fog Formation in Hypothetical LMFBR Accidents," Trans. ANS, 21, 324 (1975).
12. Golden, G.H., and J.V. Tokar, "Thermophysical Properties of Sodium," ANL-7323, Argonne National Laboratory, Argonne, Ill. (1967).
13. Han, J.T., personal communication, ORNL, April 1978.
14. Holman, J.P., "Heat Transfer," 3rd ed., McGraw-Hill, New York, 1972.
15. Hottel, H.C., and A.F. Sarofim, "Radiation Heat Transfer," McGraw-Hill, New York (1967).
16. Irvin, J.E., "Nuclear Systems Materials Handbook," Vol. 1, TID-26666, Hanford Engineering Development Laboratory, Richland, Wash.
17. McAdams, W.H., "Heat Transmission," 3rd ed., pp 66-67, McGraw-Hill, New York (1954).
18. Seigel, R., and J.R. Howell, "Thermal Radiation Heat Transfer," pp. 204-07, McGraw-Hill, New York, 1972.
19. Sparrow, E.M., and R.D. Cess, "Radiation Heat Transfer," rev. ed., Brooks and Cole, Belmont, Calif., 1970.
20. Weast, R.C., ed., "Handbook of Chemistry and Physics," 52nd ed., p. E-3, The Chemical Rubber Co., Cleveland, Ohio, 1971.

ORNL/MIT-274

INTERNAL DISTRIBUTION

1. D.A. Canonico
2. M.H. Fontana
- 3-12. J.T. Han
13. T.S. Kress
14. Yvonne Lovely
15. G.E. Moore
16. J.P. Sanders
17. H.E. Trammell

- 18-19. Central Research Library
20. Document Reference Section
- 21-23. Laboratory Records
24. Laboratory Records, ORNL R.C.
25. ORNL Patent Office
- 26-40. MIT Practice School

EXTERNAL DISTRIBUTION

41. J.E. Vivian, MIT, Cambridge, MA
42. Morgantown Energy Research Center, DOE, Morgantown, W. Va.
43. Office Asst. Mgr., Energy R&D, DOE, Oak Ridge
- 44-45. Technical Information Center

